Spontaneous Layer-Pseudospin Domain Walls in Bilayer Graphene

Xiao Li (李潇),[1] Fan Zhang,[2,*] Qian Niu,[1,3] and A. H. MacDonald[1]
[1]Department of Physics, The University of Texas at Austin, Austin, Texas 78712, USA
[2]Department of Physics, University of Texas at Dallas, Richardson, Texas 75080, USA
[3]School of Physics, International Center for Quantum Materials and Collaborative Innovation Center of Quantum Matter, Peking University, Beijing 100871, China

(Received 15 April 2014; published 12 September 2014)

Bilayer graphene is susceptible to a family of unusual broken symmetry states with spin and valley dependent layer polarization. We report on a microscopic study of the domain walls in these systems, demonstrating that they have interesting microscopic structure related to the topological character of the ordered states. We use our results to show that the metal-insulator transition temperature in bilayer graphene is reduced from mean-field estimates by thermal excitation of domain walls.

DOI: 10.1103/PhysRevLett.113.116803 PACS numbers: 73.22.Gk, 71.10.-w, 73.22.Pr, 75.60.Ch

Introduction.—Neutral bilayer graphene [1,2] and its *ABC*-stacked multilayer cousins [3–7], are attractive platforms for unconventional two-dimensional electron system physics because flat bare bands cross near their Fermi levels, and because order induces large momentum-space Berry curvatures [7] in their quasiparticle bands. Theoretical studies have identified a variety of potential broken symmetry states in neutral suspended bilayer graphene [7–33]. The band eigenstates in bilayer graphene are equal weight coherent sums of components localized in each layer, and have an interlayer phase that is strongly wave vector dependent. When lattice-scale corrections to bilayer graphene's massive Dirac model [1,2] are neglected, the broken symmetry states predicted by mean-field theory have a charged quasiparticle energy gap [7,8,10–12] and spontaneous layer polarization within each of the system's four spin-valley flavors, each giving rise to a quantized Hall contribution with magnitude e^2/h. Recent experiments [34–42] appear to rule out a competing family of nematic states [18–21], which do not have a quasiparticle gap and break rotational symmetry [43].

The theoretical expectation [7–9,16,17] is that among the gapped broken symmetry states long-range Coulomb interactions should favor the subset with no overall layer polarization. Recent experiments [42] utilize Zeeman response to an in-plane magnetic field [13] to identify the ground state as either a layer antiferromagnet [7] in which opposite spins have opposite layer polarization, or a quantum spin Hall insulator [7,16] in which layer polarization changes when either spin or valley is reversed. (In mean-field theories the former state is favored by lattice-scale exchange interactions [9].) In this Letter we present a microscopic theory of domain walls in which the sense of layer polarization of one flavor is reversed, focusing on the unusual properties associated with the ordered states' topological character. These domain walls are expected to be present in disordered bilayer graphene samples because they can be induced by spatial variation in the potential difference between layers. They also proliferate thermally above an Ising phase transition temperature, which we show is substantially suppressed relative to mean-field theory estimates.

Continuum model mean-field theory.—We first establish our notation by discussing uniform chiral symmetry breaking in bilayer graphene in terms of the ordered state quasiparticle Hamiltonians [7] suggested by mean-field calculations and renormalization group analyses [8–15]:

$$\begin{aligned}\mathcal{H}^{HF} &= \sum_{\boldsymbol{k}\alpha\beta ss'} c^\dagger_{\boldsymbol{k}\alpha s}[h_0 + h_F]c_{\boldsymbol{k}\beta s'},\\ h_0 &= -\epsilon_{\boldsymbol{k}}[\cos(2\phi_{\boldsymbol{k}})\sigma_x^{\alpha\beta} + \sin(2\phi_{\boldsymbol{k}})\sigma_y^{\alpha\beta}]\delta_{ss'},\\ h_F &= -[V_0 + V_z\sigma_z^{\alpha\alpha}\sigma_z^{\beta\beta}]\Delta^{\beta s'}_{\alpha s}. \end{aligned} \quad (1)$$

Here Greek letters label layer, s and s' label spin, $\epsilon_{\boldsymbol{k}} = (v_{\rm SL}\hbar k)^2/\gamma_1$ is the band dispersion, $v_{\rm SL}$ is the single-layer Dirac-model velocity, γ_1 is the interlayer hopping energy, $\cot\phi_{\boldsymbol{k}} = \tau_z k_x/k_y$ with $\tau_z = \pm 1$ denoting valley K or K', and $V_{0,z} = (V_s \pm V_d)/2$ is the sum and difference of the same (s) and different (d) layer interactions, which for convenience we assume to be short ranged. The order parameters $\Delta^{\beta s'}_{\alpha s} = A^{-1}\sum_{\boldsymbol{k}}\langle c^\dagger_{\boldsymbol{k}\beta s'}c_{\boldsymbol{k}\alpha s}\rangle_f$ must be determined self-consistently. Note that in using short-range interactions we are assuming that the screened Coulomb interaction range is short relative to the short-distance cutoff of the two-band continuum model, $v_{\rm SL}\hbar/\gamma_1$, but much larger than the graphene lattice constant. The form used for the mean-field Hamiltonian in Eq. (1) has been simplified by noting that the mean-field ground state has no net layer polarization, and that the mean-field interaction vertices are diagonal in layer [13]. This Hamiltonian generates a family of states differing only in the flavor dependence of the sign of interaction-generated mass terms proportional to $m_z\sigma_z$. In this Letter we concentrate on domain walls formed

within a single flavor, reserving comments on the role of spin and valley degrees of freedom to the end of the article.

The gap equation can be solved to yield an implicit solution for m_z [39]:

$$1 = \nu_0 V_s \int_0^{\gamma_1} \frac{1}{2\varepsilon}[f(-\varepsilon-\mu) - f(\varepsilon-\mu)]d\varepsilon, \qquad (2)$$

where $\nu_0 = \gamma_1/(4\pi\hbar^2 v_{\mathrm{SL}}^2)$ is the band density of states per flavor, γ_1 is the continuum model ultraviolet cutoff energy, μ is the Fermi energy, $\varepsilon = \sqrt{\epsilon_{\boldsymbol{k}}^2 + m_z^2}$, and $f(\varepsilon) = (1 + e^{\varepsilon/k_B T})^{-1}$ is the Fermi function. For charge-neutral bilayer graphene and $m_z \ll \gamma_1$, we find that the quasiparticle gap is $2m_z = 4\gamma_1 \exp(-2/V_s\nu_0)$ at zero temperature, and that m_z vanishes at $T = T_c^{\mathrm{MF}}$, where

$$T_c^{\mathrm{MF}} = e^{\gamma} m_z/\pi k_B, \qquad (3)$$

and γ is Euler's constant [39].

Microscopic theory of domain walls.—We now consider the microscopic electronic structure of the domain walls that separate regions with opposite layer-polarization signs. Because the layer-pseudospin dependent term in the band Hamiltonian is not a small correction to an otherwise pseudospin independent Hamiltonian, it is immediately clear that bilayer graphene domain walls are quite different from those of an ordinary easy-axis ferromagnet. In order to use periodic boundary conditions we must, as illustrated in Fig. 1(a), allow for two adequately separated domain walls along the direction in which we allow the sign of mass to change. We use a plane-wave expansion method to solve the spatially inhomogeneous gap equations. The interaction terms in the mean-field Hamiltonian are spatially local and can be parameterized in terms of position dependent masses $m_i(x)$ associated with the three Pauli matrices σ_i. For short-range interactions, their plane-wave matrix elements are

$$m_i(k_1', k_1) = \frac{V_s}{2A} \sum_{f\alpha\beta,\boldsymbol{q}} \langle c^{\dagger}_{k_1'+q_x,q_y,\alpha} \sigma_i^{\alpha\beta} c_{k_1+q_x,q_y,\beta} \rangle_f, \qquad (4)$$

where $i = x, y, z$, and f labels filled quasiparticle states. Note that the mass terms depend on $k_1' - k_1$ only, and that they are independent of the momentum in the y direction. The inverse Fourier transform with respect to $k_1' - k_1$ specifies $m_i(x)$.

The self-consistent mean-filed equations are readily solved in the presence of domain walls. Results for finite square simulation cells of side L are summarized in Figs. 1 and 2. A typical result for the domain wall m_z profile, plotted in Fig. 1(b), can be accurately fit to the form $m_z(x) = m_0 \tanh[(x - x_0)/\sqrt{2}\xi]$, where $2m_0$ is the quasiparticle gap and x_0 is the position of the domain wall center. As illustrated in Fig. 2(c), the energy cost of a domain wall

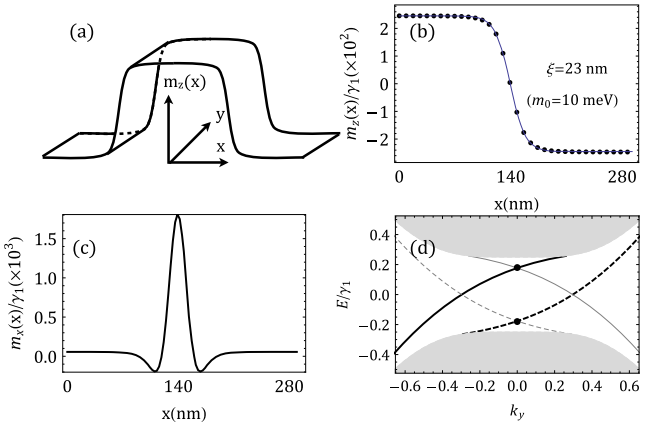

FIG. 1 (color online). (a) Schematic summary of our domain wall calculations. Two domain walls are oriented along the y direction and the mass changes sign along the x direction. (b),(c) Typical mean-field solutions for $m_z(x)$ and $m_x(x)$ variation across a domain wall. Note the different scales in (b) and (c). (d) Energy spectrum of a model with sharp domain walls. The gray area is the bulk continuum. Black and gray colors are used to distinguish chiral states localized at the domain walls which propagate in opposite directions, while solid and dashed lines are used to distinguish states with $\langle \sigma_x \rangle < (>) 0$. The two black dots identify the states with $E = \pm|m_0|/\sqrt{2}$.

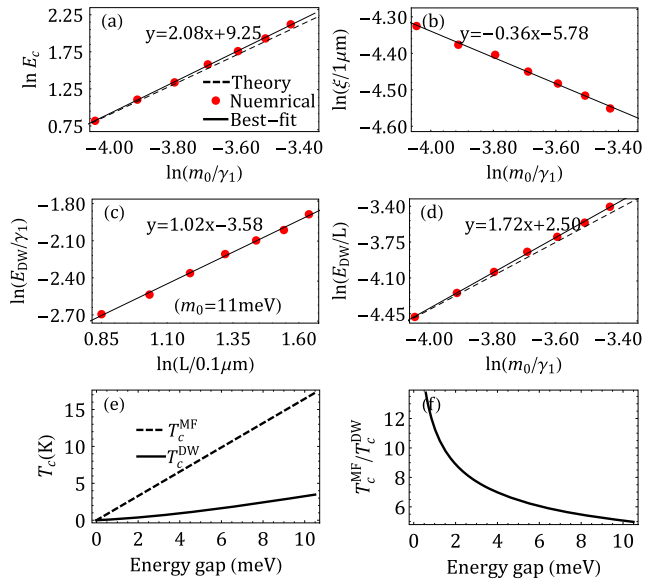

FIG. 2 (color online). Microscopic domain wall properties for square simulation cells with side L and a uniform energy gap $2m_0$. In these figures, red dots are numerical data, while the thin solid lines are power-law fits. (a) Condensation energy E_c of bilayer graphene (in units $\gamma_1/\mu\mathrm{m}^2$) as a function of m_0. The dashed line is obtained from microscopic calculations. (b) Domain wall width ξ as a function of m_0. (c) Domain wall energy E_{DW} as a function of L. (d) Domain wall surface tension $J \equiv E_{\mathrm{DW}}/L$ (in units of $\gamma_1/0.1\ \mu\mathrm{m}^2$) as a function of m_0. The dashed line is the Ginzburg-Landau theory prediction for the domain wall surface tension. (e) and (f) Comparison of the collective (T_c^{DW}) and mean-field (T_c^{MF}) critical temperatures.

$E_{\rm DW}$ in our numerical calculation is accurately proportional to L, indicating that finite-size effects are not playing a large role. Figures 2(d) and 2(b) illustrate our finding that the domain wall energy per unit length (the two-dimensional *surface tension*) $J = E_{\rm DW}/L$ and the domain wall width ξ have power-law dependences on the uniform system mass m_0. An unbiased fit of numerical results to $J \sim m_0^\alpha$ and $\xi \sim m_0^\beta$ yields $\alpha = 1.72$ and $\beta = -0.36$. These values are close to expectations based on dimensional analysis as we discuss later. We conclude that the surface tension increases and the domain wall width decreases with increasing m_0.

Interlayer coherence and domain walls.—The band states of bilayer graphene are coherent combinations [2] of top and bottom layer components with an interlayer phase ϕ that is twice the momentum orientation angle $\phi_{\boldsymbol{k}}$. The m_x and m_y pseudospin magnetizations of both gapped and ungapped states therefore vanish after summing over momenta. As illustrated in Fig. 1(c), our numerical calculations have revealed that a finite net in-plane pseudospin magnetization develops inside domain walls with a magnitude typically one order smaller than m_0. The in-plane pseudospin magnetization is oriented across the domain wall, i.e., in the x direction for the geometry we have chosen. Intriguingly, the sign of m_x is the same for both kink and antikink domain walls. The appearance of these in-plane pseudospin components is a surprise since they are not an obvious consequence of the spatial dependence of m_z. For example, the uniform system m_x and m_y quasiparticle linear response to pseudospin fields in the $\hat{z}$ direction, characterized by the response functions $\chi_{xz}(\boldsymbol{q})$ and $\chi_{yz}(\boldsymbol{q})$, both vanish identically. As we explain below, the appearance of a nonzero m_x in the domain walls is related to the topological character of the ordered states.

Near a domain wall, the sign of m_z is reversed and the local value of the Hall conductivity changes by two quantized units [7,44,45], giving rise to two chiral zero modes per valley propagating along the domain wall, as illustrated in Fig. 1(d). As we now explain, we attribute the finite m_x value in the domain wall to the properties of the topological edge states it traps. At any value of k_y the mean-field Hamiltonian $\mathcal{H}$ in the presence of domain walls is invariant under simultaneous rotation by 180° around the pseudospin $\hat{x}$ axis and mirror transformation $x \to -x$ through the domain wall: $\sigma_x \mathcal{H} \sigma_x = \mathcal{H}(-\partial_x, -x)$. Here we assume that $x = 0$ is chosen to lie at the midpoint of a single domain wall. It follows that for any k_y, the two components of the eigenstates $\psi(x) = [u(x), v(x)]^T$ satisfy $v(x) = \pm u(-x)$, and, hence, that the pseudospin operator σ_x will have a nonzero expectation value near $x = 0$. Similarly since $\sigma_y \mathcal{H}(k_y) \sigma_y = -\mathcal{H}(-k_y)$, if $(u, v)^T$ is an eigenstate of $\mathcal{H}$ at k_y with eigenvalue E, then $(v, -u)^T$ is an eigenstate at $-k_y$ with eigenvalue $-E$. It follows that the two chiral states with $E = 0$ will appear at opposite values of k_y and have opposite expectation values of $\langle \sigma_x \rangle$. For example, in the case of a sharp kink, i.e., for $m_z(x) = m_0 \mathrm{sgn}(x)$, the chiral states at $k_y = 0$ have $E = \pm |m_0|/\sqrt{2}$ (lying in the gap) and $\langle \sigma_x \rangle = \mp 1$. Although the edge states are not fully polarized in the general case, states within a given chiral state branch have nonzero values of $\langle \sigma_x \rangle$ with a common sign and the edge state occupations are generically different for any position of the chemical potential within the uniform-state mass gap.

Typical behavior is illustrated in Fig. 1(d). The dashed and solid edge state branches have different signs of $\langle \sigma_x \rangle$ and different occupations. As a consequence, $m_x(x)$ exhibits a positive peak at each domain wall center. This in-plane pseudospin magnetization is independent of the domain wall sign and valley index, and thus survives summation over flavors for any gapped broken symmetry state that breaks chiral symmetry within flavors [7]. We note that this nonlinear response also arises near electric field driven domain walls [44–52] and layer stacking domain walls [45–47].

Ising critical temperature estimate.—We now utilize our numerical results for domain wall properties to estimate the critical temperature $T_c^{\rm DW}$ above which domain walls nucleated by thermal fluctuations proliferate and Ising long-range order within flavors is lost. For this purpose, we follow a common physical argument [53] which compares the energy cost associated with domain wall nucleation with the corresponding entropic free energy gain. The energy cost to form a domain wall with perimeter P in the uniform state is JP, whereas the entropy is $k_B \ln C_P$. Here C_P is the number of distinct closed-loop nonintersecting P/W-step walks. For domain walls of width ξ, $W \sim 2\sqrt{2}\xi$ [53] is the minimum distance over which a domain wall can change direction and $C_P = (1+\sqrt{2})^{P/W}$ [53]. It then follows that for temperatures above $T_c^{\rm DW} = WJ/[k_B \ln(1+\sqrt{2})]$, the proliferation of domains separating regions with different layer polarization signs is thermodynamically favored and long-range order is lost. Combining our numerical results for ξ and J yields

$$\frac{k_B T_c^{\rm DW}}{m_0} = \frac{0.64}{\ln(1+\sqrt{2})} (m_0/\gamma_1)^{\alpha+\beta-1}. \tag{5}$$

Since $\alpha + \beta - 1 > 0$ and $m_0 \ll \gamma_1$, we conclude that $k_B T_c^{\rm DW} \ll m_0$.

We have so far ignored fermionic thermal fluctuations which produce particle-hole excitations and would limit the critical temperature if the domain wall energy was very large. Because the mean-field theory gap equation is identical to that of BCS theory, it implies a critical temperature limit that is proportional to m_0. As illustrated in Figs. 2(e) and 2(f), the ratio $T_c^{\rm MF}/T_c^{\rm DW}$ decreases with increasing m_0, in agreement with Eq. (5). Noting that $\gamma_1 \sim 400$ meV and that experimental [39] values of m_0 in bilayer graphene are always smaller than 4 meV, we conclude that the temperature to which spontaneous layer polarization order survives is limited in practice by domain wall nucleation.

Phenomenological theory of domain walls.—The domain wall shape found in our numerical calculations

is consistent [53,54] with the Ising-order Ginzburg-Landau-theory energy functional

$$F = \int d^2\vec{r}\left[\frac{c}{2}(\nabla m_z)^2 + \mathcal{V}[m_z(x)] - E_c\right], \qquad (6)$$

where $\mathcal{V}[m_z] = -rm_z(x)^2/2 + um_z(x)^4$ with both r and u positive, and $E_c = -r^2/16u$ is the condensation energy per unit area of a ground state with uniform m_z. We include the constant E_c in this expression so that the minimum value of F, which occurs for constant masses $m_z^* = \pm m_0 = \pm(r/4u)^{1/2}$, is zero. For a single domain wall configuration in which $m_z \to \pm m_0$ for $x \to \pm\infty$, the functional [Eq. (6)] is minimized by $m_z(x) = \pm m_0 \tanh[(x - x_0)/\sqrt{2}\xi]$ with $\xi = \sqrt{c/r}$. The close agreement between our numerical domain wall shapes and this analytic expression demonstrates that the Ginzburg-Landau theory for spontaneously gapped states in bilayer graphene is of the standard Ising magnetism form, in spite of the unusual microscopic physics. The Ginzburg-Landau model reproduces microscopic values for m_0, ξ, and E_c when we set $c = 4E_c\xi^2/m_0^2$, $r = 4E_c/m_0^2$, and $u = E_c/m_0^4$. (Note that m_0 is strongly temperature dependent for a given value of the interaction strength.) In Fig. 2(a) we demonstrate that the Ginzburg-Landau theory expression for the domain wall surface tension $J = 8\sqrt{2}\xi E_c/3$ agrees accurately with our microscopic calculations, and that the power laws relating ξ and J to the microscopic gap satisfy $\alpha - \beta = 2$, also in agreement with the Ginzburg-Landau theory.

Discussion.—It is instructive to compare spontaneously gapped bilayer graphene with BCS superconductors. In both cases mean-field theory predicts a critical temperature that is linear in the gap parameter m_0. Fluctuation effects differ qualitatively in the two cases, however, in the first place because of the difference between the order parameter dimensions. In superconductors, the excitations whose proliferation limits the critical temperature are vortices rather than domain walls. Additionally, the free fermion dispersion is linear near the Fermi energy in the superconductor case but *quadratic* in bilayer graphene. As a result, the coherence length in superconductors is related to the gap Δ by $\xi \sim \hbar v_{\rm SL}/\Delta$, and the collective fluctuation limit on the critical temperature must therefore exceed the nucleation energy of a vortex, i.e., $k_B T_c \sim E_c\xi^2 \sim \varepsilon_F$ which is independent of and much larger than the mean-field critical temperature estimate. A similar estimate of the collective limit on T_c can be obtained by appealing to Kosterlitz-Thouless theory. These considerations explain why critical temperatures of weakly disordered superconducting thin films are still accurately predicted by mean-field theory, even though the phase transition is ultimately of Kosterlitz-Thouless character. In bilayer graphene, on the other hand, the relationship between ξ and the gap can be estimated using $m_0 \sim (\hbar v_{\rm SL}/\xi)^2/\gamma_1$. This estimate yields $\beta = -0.5$, in rough agreement with the value $\beta = -0.36$ obtained by fitting our numerical results. It follows that for bilayer graphene, collective fluctuations limit the critical temperature to a value that is substantially lower than the mean-field-theory estimate. Unlike the case of superconductors, in bilayer graphene thermal fluctuations in the order parameter configuration play an important role in limiting the critical temperature.

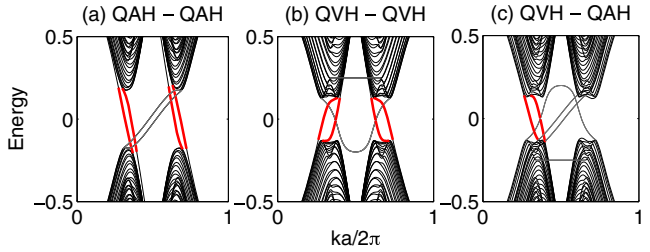

FIG. 3 (color online). Tight-binding calculation of distinct domain wall zero-mode patterns in gapped bilayer graphene samples with spin-rotational invariance. The red lines denote the zero modes localized at domain walls between (a) two QAH regions with opposite total Hall conductance, (b) two QVH regions with opposite layer polarization, and (c) a QVH and a QAH region. The gray lines represent the edge states on the outermost zigzag boundaries.

When the four spin-valley flavors are taken into account, the $2^4 = 16$ gapped broken symmetry states that are close in energy [9] can be classified into five distinct phases [7]. This in turn leads to 16 distinct types of domain walls [55]. In Fig. 3 we illustrate the cases [55] in which spin rotational invariance is not broken, and only the quantum valley Hall (QVH) state and quantum anomalous Hall (QAH) state are allowed. Because in the absence of intervalley scatterings the valley-projected Chern numbers are quantized [7,44,45,52] to ± 1, all domain walls support edge states, as shown in Fig. 3. States in which spin-rotational invariance is also broken can be similarly analyzed. Each of the 16 types of domain wall hosts a Luttinger liquid [56] with distinct properties. Our work therefore suggests that large-area bilayer graphene gapped states should exhibit interesting transport anomalies [57]. Similar phenomena will occur in thicker *ABC*-stacked few-layer [7] graphene systems which have larger spontaneous gaps [36,37] and more robust domain walls.

X. L. acknowledges Zhenhua Qiao, Hua Chen, and Ming Xie for helpful technical advice and is supported by NBRPC (No. 2012CB921300 and No. 2013CB921900) and NSFC (No. 91121004) during his visit at Peking University. F. Z. is indebted to B. J. Wieder, C. Kane, and E. Mele for helpful discussions and has been supported by UT Dallas research enhancement funds. Q. N. is supported in part by DOE-DMSE (No. DE-FG03-02ER45958) and the Welch Foundation (No. F-1255). A. H. M. is supported by the Welch Foundation under Grant No. TBF1473 and by the DOE Division of Materials Sciences and Engineering under Grant No. DE-FG03-02ER45958.

*zhang@utdallas.edu

[1] A. H. Castro Neto, F. Guinea, N. M. R. Peres, K. S. Novoselov, and A. K. Geim, Rev. Mod. Phys. **81**, 109 (2009).
[2] E. McCann and V. I. Fal'ko, Phys. Rev. Lett. **96**, 086805 (2006).
[3] H. Min and A. H. MacDonald, Phys. Rev. B **77**, 155416 (2008).
[4] M. Koshino and E. McCann, Phys. Rev. B **80**, 165409 (2009).
[5] F. Zhang, B. Sahu, H. Min, and A. H. MacDonald, Phys. Rev. B **82**, 035409 (2010).
[6] X. Li, Z. Qiao, J. Jung, and Q. Niu, Phys. Rev. B **85**, 201404 (R) (2012).
[7] F. Zhang, J. Jung, G. A. Fiete, Q. Niu, and A. H. MacDonald, Phys. Rev. Lett. **106**, 156801 (2011).
[8] H. Min, G. Borghi, M. Polini, and A. H. MacDonald, Phys. Rev. B **77**, 041407(R) (2008).
[9] J. Jung, F. Zhang, and A. H. MacDonald, Phys. Rev. B **83**, 115408 (2011).
[10] F. Zhang, H. Min, M. Polini, and A. H. MacDonald, Phys. Rev. B **81**, 041402(R) (2010).
[11] R. Nandkishore and L. Levitov, Phys. Rev. Lett. **104**, 156803 (2010).
[12] F. Zhang, H. Min, and A. H. MacDonald, Phys. Rev. B **86**, 155128 (2012).
[13] F. Zhang and A. H. MacDonald, Phys. Rev. Lett. **108**, 186804 (2012).
[14] A. H. MacDonald, J. Jung, and F. Zhang, Phys. Scr. **T146**, 014012 (2012).
[15] M. M. Scherer, S. Uebelacker, and C. Honerkamp, Phys. Rev. B **85**, 235408 (2012).
[16] R. Nandkishore and L. Levitov, Phys. Rev. B **82**, 115124 (2010).
[17] X. Z. Yan and C. S. Ting, Phys. Rev. B **86**, 125438 (2012).
[18] O. Vafek and K. Yang, Phys. Rev. B **81**, 041401(R) (2010).
[19] Y. Lemonik, I. L. Aleiner, C. Toke, and V. I. Fal'ko, Phys. Rev. B **82**, 201408(R) (2010).
[20] A. S. Mayorov, D. C. Elias, M. Mucha-Kruczynski, R. V. Gorbachev, T. Tudorovskiy, A. Zhukov, S. V. Morozov, M. I. Katsnelson, V. I. Fal'ko, A. K. Geim, and K. S. Novoselov, Science **333**, 860 (2011).
[21] A. M. Cook, C. Hickey, and A. Paramekanti, arXiv:1405.5880 [Phys. Rev. B. (to be published)].
[22] T. C. Lang, Z. Y. Meng, M. M. Scherer, S. Uebelacker, F. F. Assaad, A. Muramatsu, C. Honerkamp, and S. Wessel, Phys. Rev. Lett. **109**, 126402 (2012).
[23] R. Nandkishore and L. Levitov, Phys. Rev. B **82**, 115431 (2010).
[24] O. Vafek, Phys. Rev. B **82**, 205106 (2010).
[25] M. Trushin and J. Schliemann, Phys. Rev. Lett. **107**, 156801 (2011).
[26] M. Trushin and J. Schliemann, New J. Phys. **14**, 095005 (2012).
[27] M. Kharitonov, Phys. Rev. B **86**, 195435 (2012).
[28] E. V. Gorbar, V. P. Gusynin, V. A. Miransky, and I. A. Shovkovy, Phys. Rev. B **86**, 125439 (2012).
[29] R. E. Throckmorton and O. Vafek, Phys. Rev. B **86**, 115447 (2012).
[30] V. Cvetkovic, R. E. Throckmorton, and O. Vafek, Phys. Rev. B **86**, 075467 (2012)
[31] Y. Lemonik, I. L. Aleiner, and V. I. Fal'ko, Phys. Rev. B **85**, 245451 (2012).
[32] X. Z. Yan and C. S. Ting, Phys. Rev. B **86**, 235126 (2012); **88**, 045410 (2013).
[33] L. Zhu, V. Aji, and C. M. Varma, Phys. Rev. B **87**, 035427 (2013).
[34] J. Martin, B. E. Feldman, R. T. Weitz, M. T. Allen, and A. Yacoby, Phys. Rev. Lett. **105**, 256806 (2010).
[35] R. T. Weitz, M. T. Allen, B. E. Feldman, J. Martin, and A. Yacoby, Science **330**, 812 (2010).
[36] W. Bao, L. Jing, J. Velasco, Jr., Y. Lee, G. Liu, D. Tran, B. Standley, M. Aykol, S. B. Cronin, D. Smirnov, M. Koshino, E. McCann, M. Bockrath, and C. N. Lau, Nat. Phys. **7**, 948 (2011).
[37] Y. Lee, D. Tran, K. Myhro, J. Velasco, Jr., N. Gillgren, C. N. Lau, Y. Barlas, J. M. Poumirol, D. Smirnov, and F. Guinea, arXiv:1402.6413.
[38] F. Freitag, J. Trbovic, M. Weiss, and C. Schönenberger, Phys. Rev. Lett. **108**, 076602 (2012).
[39] J. J. Velasco, L. Jing, W. Bao, Y. Lee, P. Kratz, V. Aji, M. Bockrath, C. Lau, C. Varma, R. Stillwell, D. Smirnov, F. Zhang, J. Jung, and A. MacDonald, Nat. Nanotechnol. **7**, 156 (2012).
[40] W. Bao, J. Velasco, Jr., F. Zhang, L. Jing, B. Standley, D. Smirnov, M. Bockrath, A. H. MacDonald, and C. N. Lau, Proc. Natl. Acad. Sci. U.S.A. **109**, 10802 (2012).
[41] A. Veligura, H. J. van Elferen, N. Tombros, J. C. Maan, U. Zeitler, and B. J. van Wees, Phys. Rev. B **85**, 155412 (2012).
[42] F. Freitag, M. Weiss, R. Maurand, J. Trbovic, and C. Schönenberger, Phys. Rev. B **87**, 161402(R) (2013).
[43] G. Dávid, P. Rakyta, L. Oroszlány, and J. Cserti, Phys. Rev. B **85**, 041402(R) (2012).
[44] I. Martin, Y. M. Blanter, and A. F. Morpurgo, Phys. Rev. Lett. **100**, 036804 (2008).
[45] F. Zhang, A. H. MacDonald, and E. J. Mele, Proc. Natl. Acad. Sci. U.S.A. **110**, 10546 (2013).
[46] J. S. Alden, A. W. Tsen, P. Y. Huang, R. Hovden, L. Brown, J. Park, D. A. Muller, and P. L. McEuen, Proc. Natl. Acad. Sci. U.S.A. **110**, 11256 (2013).
[47] A. Vaezi, Y. Liang, D. H. Ngai, L. Yang, and E. A. Kim, Phys. Rev. X **3**, 021018 (2013).
[48] W. Yao, S. A. Yang, and Q. Niu, Phys. Rev. Lett. **102**, 096801 (2009).
[49] J. Jung, F. Zhang, Z. Qiao, and A. H. MacDonald, Phys. Rev. B **84**, 075418 (2011).
[50] Z. Qiao, J. Jung, Q. Niu, and A. H. MacDonald, Nano Lett. **11**, 3453 (2011).
[51] M. Zarenia, J. M. Pereira, Jr., G. A. Farias, and F. M. Peeters, Phys. Rev. B, **84**, 125451 (2011).
[52] J. Li, I. Martin, M. Buttiker, and A. F. Morpurgo, Nat. Phys. **7**, 38 (2011).
[53] P. M. Chaikin and T. C. Lubensky, *Principles of Condensed Matter Physics* (Cambridge University Press, Cambridge, England, 2000), reprint ed.
[54] M. Tinkham, *Introduction to Superconductivity* 2nd ed. (Courier Dover Publications, New York, 2012).
[55] F. Zhang, J. Jung, and A. H. MacDonald, J. Phys. Conf. Ser. **334**, 012002 (2011).
[56] M. Killi, T. C. Wei, I. Affleck, and A. Paramekanti, Phys. Rev. Lett. **104**, 216406 (2010).
[57] B. J. Wieder, F. Zhang, and C. L. Kane (unpublished).